VARIOUS DAMAGE DETECTION IN ADVANCED GRID STRUCTURE BY MONITORING OF GUIDED WAVES WITH EMBEDDED FIBER BRAGG GRATING SENSORS

Masataro AMANO*, Takeo ARAI* and Nobuo TAKEDA*
***The University of Tokyo, Department of Advanced Energy, **Company2**

Keywords: *Advanced Grid Structure (AGS), Structural Health Monitoring (SHM), Longitudinal waves, Flexural waves, Fiber Bragg grating (FBG)*

Abstract

The authors have tried to construct a structural health monitoring (SHM) system to identify damage in composite grid structure called Advanced Grid Structure (AGS). Two types of guided waves, compressional and flexural waves were propagated along ribs of AGS to detect various damage types. Those waves were measured with fiber Bragg grating (FBG) sensors network embedded in AGS. With this SHM system, the authors had reported some possibilities of detecting two types of damages. In this paper, we applied this system to all possible damage types. The results were summarized to clarify which damage types could be detected with this system. Especially, the authors applied two types of damage diagnosis methods with compressional and flexural waves, respectively. Those possibilities were classified by the two methods. Some possibilities were verified experimentally or computationally.

1 Introduction

Carbon fiber reinforced plastic (CFRP) has been considered as a major material for aerospace structures because it has high specific strength and modulus in fiber direction. Application of CFRP to those structures dramatically reduces the weight of those structures and the cost for fabrication, which are indispensable in aerospace field. However, the specific strength and modulus of CFRP in fiber transverse direction is comparatively low. Therefore, CFRP is generally used as laminates or woven type composites, which results in occurrence of various complicated damage features. As a result, safety factors have been kept high compared to metallic materials and the weight saving do not have fully been achieved.

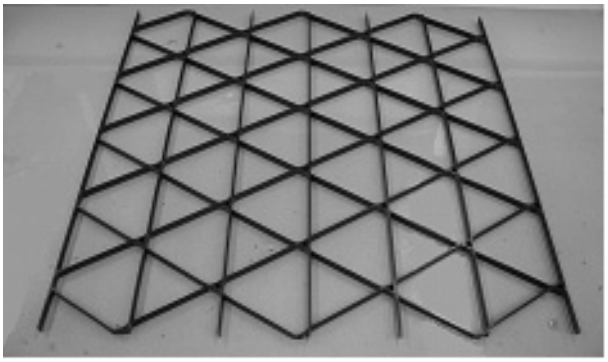

Fig. 1. Advanced grid structure (AGS) made of CFRP.

In recent years, a new type of CFRP structure has been accepted as a possible solution to the problems associated with lamination. It is a grid structure made of CFRP unidirectional composites, named as an advanced grid structure (AGS). Figure 1 shows an example of AGS. AGS is defined as trussed structures whose ribs are made of Carbon fiber reinforced plastic (CFRP). It has several advantages compared with other conventional structures[1]. The authors had reported one possible method of SHM of AGS by monitoring of static strain distribution with embedded FBG sensors network in AGS [2]. Moreover, another possible SHM system by monitoring of two types of guided waves, compressional and flexural waves, had been proposed in our last work [4]. There are two main advantages to the previous SHM system. The first one is that the guided wave system does not require inspection loading. Therefore, this system is simple for testing. The second one is that the system does not require baseline data. Therefore, several errors related to measurement under different

environmental conditions are negligible. Moreover, those waves can be measured with an innovative measurement system based on the same strain measurement system which we have already been constructed [2], which are summarized in Section 2. This measurement system was composed of fibre Bragg grating (FBG) sensors [3]. FBG sensor is a kind of optical strain sensors that consists of a periodic refractive index change formed in the core of an optical fibre. When a broadband light propagates into an FBG sensor, only narrow component at Bragg wavelength λ_0 is reflected which corresponds to grating period Λ and effective refractive index n as,

$$\lambda_0 = 2n\Lambda \qquad (1)$$

FBG sensors have often been applied for health monitoring of CFRP[5]. The FBG sensors were multiplexed into few optical fibres and embedded the sensors into all ribs of AGS (one rib has one FBG). Since all ribs of AGS are composed of CFRP unidirectional laminates, all optical fibres can be easily embedded parallel to carbon fibres. Therefore, the embedment does not deteriorate mechanical properties of CFRP and realizes permanent strain distribution measurement.

With the system, two types of damage diagnosis methods were proposed in this research and were experimentally and analytically verified.

2 Concept of Damage Detection

2.1 System Outlines

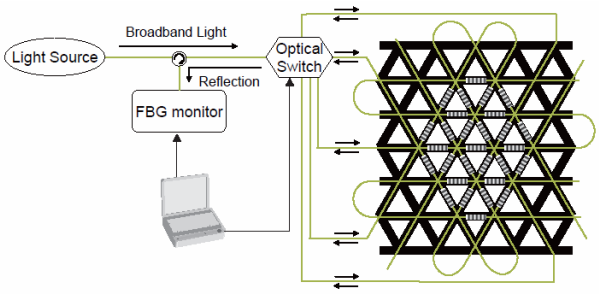

Fig. 2. Schematic of strain measurement system with multiplexed FBG sensors embedded in Advanced Grid Structure (AGS).

Figure 2 represents a schematic of the SHM system. Some multiplexed FBG sensors are embedded along the corresponding ribs in AGS. Each FBG is embedded in the center of a rib parallel to carbon fiber. A broadband light propagates all optical fiber through an optical switch. When the light reaches every FBG sensor, a narrow band light determined from its average specific refractive index n_i and grating period Λ_i according to Eq. 1 is reflected from the FBG. Therefore, every FBG reflects a narrow band light with different wavelength λ_i. Those narrow band lights are introduced into FBG monitor through the optical switch again and their current wavelengths are measured.

When the AGS deforms, the embedded FBG sensors are strained and the wavelengths of their reflecting lights change according to Eq. 2 as,

$$\frac{\Delta\lambda_i}{\lambda_i} = \left[1 - \frac{n_i^2}{2}\left\{p_{12} - \nu\left(p_{11} + p_{12}\right)\right\}\right] \times \varepsilon_i^{OF}$$

$$\Leftrightarrow \varepsilon_i^{OF} = \frac{1}{\left[1 - \frac{n_i^2}{2}\left\{p_{12} - \nu\left(p_{11} + p_{12}\right)\right\}\right]\lambda_i} \times \Delta\lambda_i \qquad (2)$$

$$\Leftrightarrow \varepsilon_i^{OF} = C_i \times \Delta\lambda_i$$

Since every FBG has different n_i and Λ_i, we can measure strains at all ribs simultaneously.

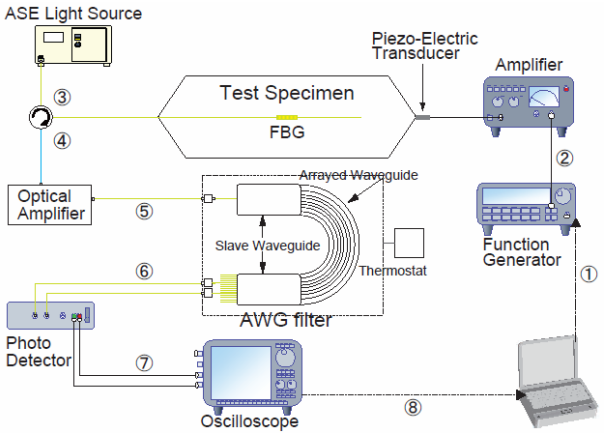

Fig. 3. Elastic wave measurement system with embedded FBG sensors.

Based on this basic concept of strain measurement system with multiplexed FBG sensors embedded in AGS, a following elastic wave measurement system was proposed. Figure 3 represents the schematic of this system[6]. The measuring processes of elastic waves are as follows,

1. Generate waveform with PC and send it to Function Generator.
2. Generate corresponding voltage signal with the function generator and amplify it by electrical amplifier. The attached piezoelectric transducer accelerates AGS and generates elastic waves.

3. The elastic waves are measured with the embedded FBG sensors as the historical data of rib longitudinal strains.
4. All FBGs reflect several narrow band lights. They are amplified by the optical amplifier.
5. With an arrayed waveguide grating (AWG) filter[7][8], the change of wavelength of reflected light is transfered to optical intensity signal. A photo detector changes the intensity signal to a voltage signal.
6. An oscilloscope measures this voltage signal, whose waveform directly corresponds to the waveform of the elastic wave signal measured with embedded FBG sensors.

However, since strains caused by elastic waves are small, all signals are buried into electrical noises from several equipments. Therefore, in this measurement, generation and measurement of elastic waves are repeated and averaged in order to remove electrical noises. Moreover, for the purpose of atmosphere stabilization, thermo regulator controls temperature of AWG filter.

2.2 Methods of Damage Detection

We had proposed following two damage diagnosis systems with compressional and flexural waves based on their characteristics [4]. These proposals are based on the following assumption that the mechanical characteristics of all ribs are the same. This means that there is no difference between all ribs in AGS after its fabrication.

Figures 4 and 5 illusrate concepts of damage diagnosis strategies with compressional and flexural waves, respectively.

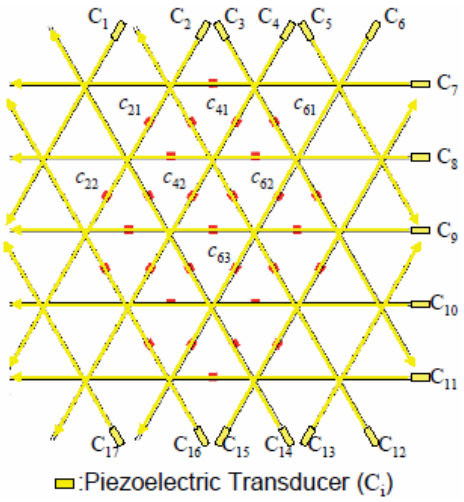

Fig. 4. Schematic of damage diagnosis method by compressional wave.

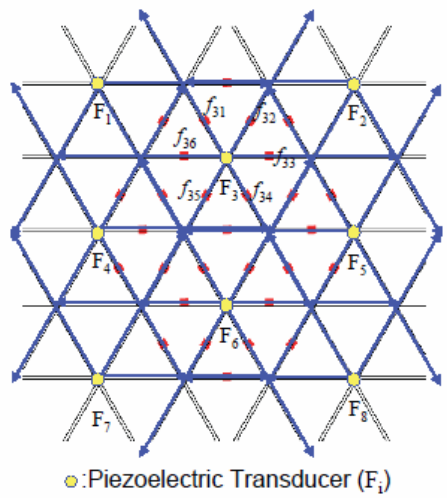

Fig. 5. Schematic of damage diagnosis method by flexural wave.

Compressional wave is used for long span and directional damage diagnosis. We diagnose every path (i) with one corresponding piezoelectric transducer (C_i) attached at the edge of the path i as shown in Fig.4. In every path i, there are some FBG sensors (c_{ij}) embedded at equal intervals. When all C_i generate the same compressional waves, all c_{ij} which located in an equal distance (j) should measure the same waveforms, especially for the first arrival waves.

For example, in Fig.4, if C_2, C_4 and C_6 generate the same compressional waves, the waveforms of first arrival waves measured by c_{21}, c_{41} and c_{61}, or c_{22}, c_{42} and c_{62} should be the same. However, if there is a damage between c_{21} and c_{22}, although the waveforms of first arrival waves measured by c_{21}, c_{41} and c_{61}, the waveform of first arrival wave measured by c_{22} should be different from those measured by c_{42} and c_{62}. From this result, we could conclude that damage appeared on line i and the damage location was between c_{21} and c_{22}. This is the basic concept of our proposed damage diagnosis method with compressional waves.

Subsequently, flexural wave is used for two dimensional damage diagnosis. Therefore, we attach piezoelectric transducers (F_i) arranged at intervals of three ribs as shown in Fig.5. Six FBG sensors embedded around F_i are named as f_{ij} ($j = 1, \cdots, 6$). When an F_i generates a flexural wave, six waveforms measured at f_{ij} ($j = 1, \cdots, 6$) should be the same with each other, especially for their first arrival waves.

For example, in Fig. 5, if F_3 generates a flexural wave, the waveforms of first arrival waves

measured by f_{3j} ($j = 1, \cdots, 6$) should be the same. However, if there is a damage between F_3 and f_{31}, the waveform of first arrival wave measured by f_{31} must be different from those measured by other FBG sensors f_{3j} ($j = 2, \cdots, 6$). From this result, we could conclude that damage appeared between F_3 and f_{31}. This is the basic concept of our proposed damage diagnosis method with flexural waves.

In following sections 3 and 4, we construct specific damage diagnosis methods for both compressional and flexural waves to detect several specific damage types. The validities of those methods are verified experimentally and analytically.

3 Damage Diagnoses with Compressional Wave

3.1 Rib Crack Detection

In this section, we attempt to detect a specific damage type, fiber break induced rib crack as shown in Fig. 6, by monitoring of compressional waves. Figure 7 represents a test configuration. An AGS was used as the specimen, whose size is represented in Table 1. This specimen has attached FBG sensors as illustrated in Fig. 7. We chose two different paths in the specimen. In both paths, there were a piezoelectric transducer whose resonance frequency was 80kHz and FBG sensors. The transducer was attached on the surface of the end of this specimen as shown in Figure 7. In addition, four multiplexed FBG sensors from 1 to 4 were attached on lower surfaces of four ribs in each path. Directions of those sensors were parallel to rib longitudinal directions.

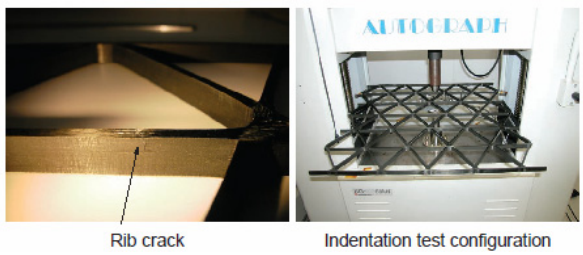

Fig. 6. Three point bending test configurations for generating a fiber break on top surface.

Table 1. Sizes of AGS specimen.

A	526.8	±0.2	mm
B	550.9	+0.16, -0.14	mm
a	105.0	±0.1	mm
b	182.1	+1.39, -1.01	mm
l	93.2	+1.41, -1.09	mm
t	1.8	+0.33, -0.27	mm
h	9.7	+0.34, -1.04	mm

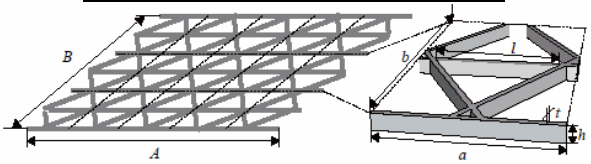

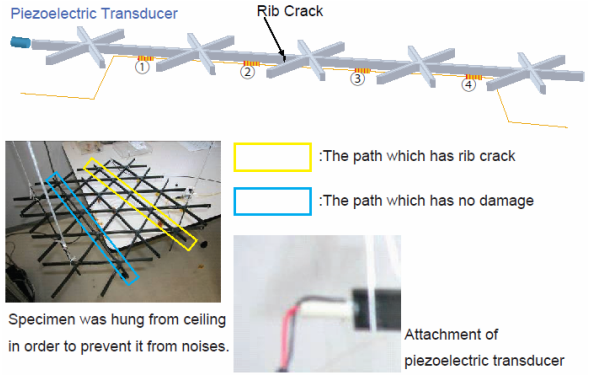

Fig. 7. Schematic of damage detection test with compressional waves generated at attached piezo-electric transducer. Each lower surface of ribs had one attached FBG sensor, which were multiplexed into one optical fiber.

In the experiment, one of the two paths was chosen and the rib crack was generated in the path under three point bending load as shown in Fig. 6. The location of this crack is shown in Fig. 7. Then, compressional waves were measured at four FBGs in both paths and compared with each other for the maximum amplitudes of their first arrival waves (V_p).

Figure 8 shows the result of this experiment. In this figure, two graphs represent measured waves at 2 and 3. In those graphs, dotted lines and continuous lines represent received waves and their envelopes, respectively. The envelopes were calculated with Hilbert transform. As shown in this figure, although V_p s measured at 2 (forward from the damage) were the same, V_p s measured at 3 were different. The V_p in the path which has damage was smaller than that in the other path. This is because there is a

discontinuous surface in the path caused by the rib crack. Since surfaces of the crack intercepts transmission of compressional wave energy, V_p became smaller than others. Therefore, if the V_p measured in a path is smaller and statistically unusual from others, we can determine that there is a rib cracking in the path.

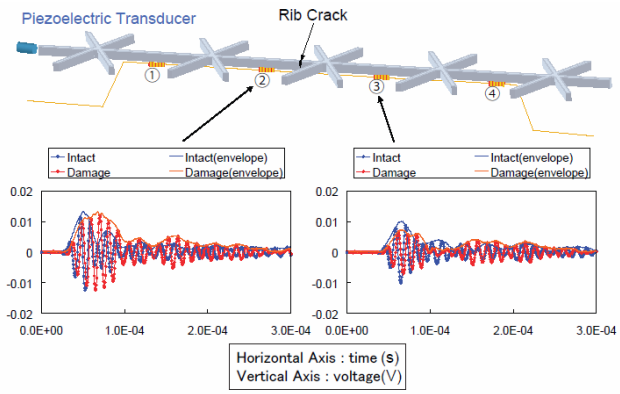

Fig. 8. Change of the maximum amplitudes of first arrival compressional waves induced by fiber break as illustrated. The amplitudes measured at 3 reduced according to the occurrence of fiber break.

3.2 Analytical Verification

The previous experimental result was analytically verified with finite element analysis (FEA). In this research, a dynamic explicit method was used for the calculation with a commercial software, ABAQUS (ABAQUS Inc.). Figure 9 represents the calculation model. In the model, ribs and cross sections were modeled with 3D brick elements with 8 nodes. The thickness, width and longitudinal directions of ribs were divided into 6, 2 and 20 elements, respectively. Except, since the cross sections were mechanically and structurally complex, they were divided more precisely than other parts as shown in Fig.9. And near the cross sections, in order to adjust the precisenesses between rib and cross section, those areas were modeled with triangular pole elements. The material properties were summarized in Table 2. Rib cracking was modeled with double nodes as shown in Fig. 10 to represent generation of a discontinuous surface.

In the beginning of the calculation, dynamic pressure was applied at the end of the paths with the maximum pressure P=2.7*10^4 (Pa). The frequency of this compressional wave was 81 kHz. The received waveforms were evaluated as the history of rib axial strain E_{11} defined at locations where FBG sensors were assumed to be embedded. After the calculation, envelopes of the received waveforms were calculated and V_p s were compared.

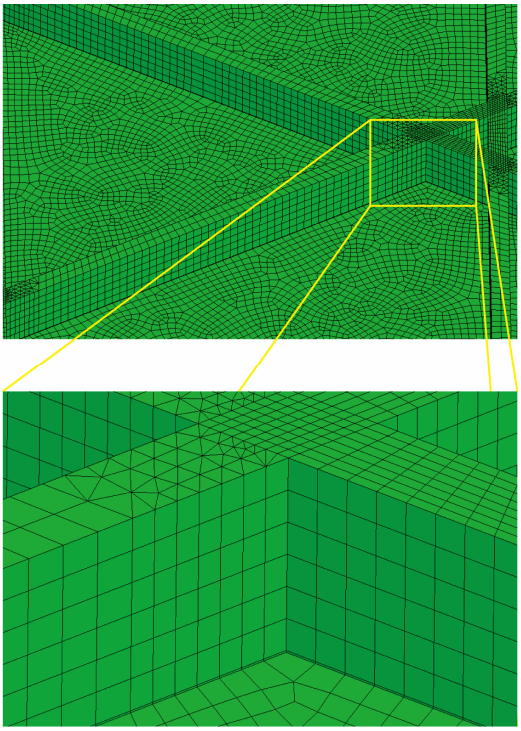

Fig. 9. FEA modeling.

Table 2. Mechanical properties of CFRP used for the calculation.

E_{11}	149	GPa
E_{22}	7.65	GPa
G_{12}	3.25	GPa
G_{23}	2.57	GPa
ν_{12}	0.281	
ν_{23}	0.49	
ρ	1500	kg/m^3

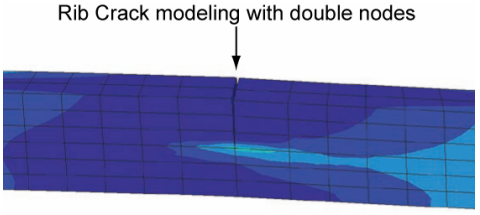

Fig. 10. Modeling of fiber break induced rib cracking in FEA.

Fig. 11 represents the calculated results. In this figure, all graphs from 1 to 4 were the received

waveforms calculated at four different locations. As shown in these graphs, although V_p s measured at 2 were the same, those measured at 3 were different. The V_p measured in the damaged path was smaller than that in the no damage path. This tendency was the same as experimental result. Therefore, the fact that the discontinuous surface in the path caused by the rib cracking intercepts the transmission of compressional wave energy was analytically verified.

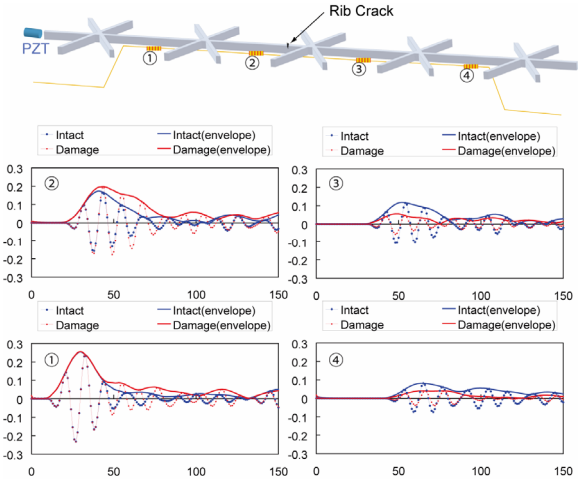

Fig. 11. Result of the calculation for discussing the effect of fiber break induced rib cracking toward compressional wave propagation in AGS.

4 Damage Diagnoses with Flexural Wave

In this section, we subsequently attempt to detect another specific damage type, debonding between ribs and skin as shown in Fig. 12, by monitoring of flexural waves.

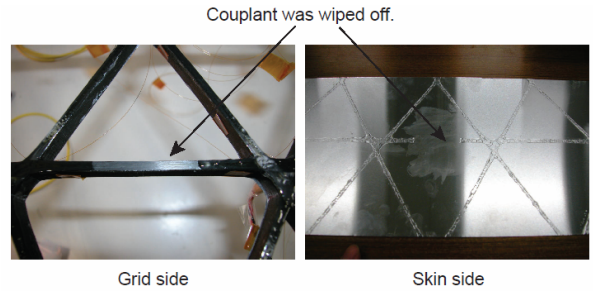

Fig. 12. Method for introducing non-adhesion area between lattice and skin by removing couplant.

Figure 13 represents a test configuration. Specimen is the same as used in Section 3. A piezoelectric transducer whose resonance frequency was 40kHz and FBG sensors was attached on top and bottom surfaces of the specimen as shown in Figure 13. In addition, six multiplexed FBG sensors from 1 to 6 were attached on lower surfaces of six ribs around the transducer. Directions of those sensors were parallel to rib longitudinal directions.

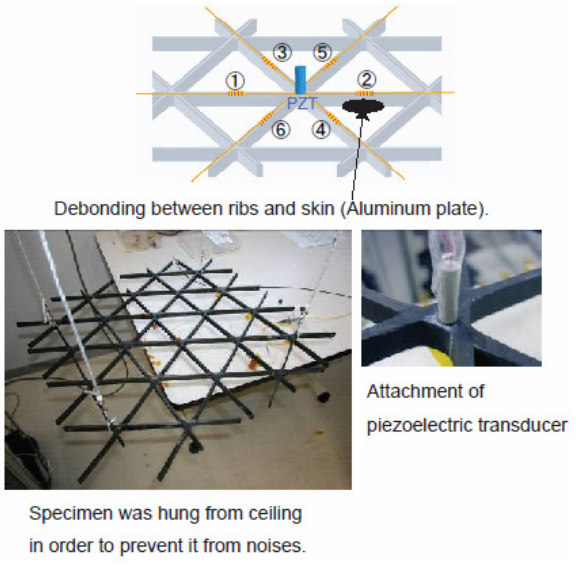

Fig. 13. Schematic of damage detection test with flexural waves generated at attached piezo-electric transducer. Each lower surfaces of ribs had one attached FBG sensor, which were multiplexed into one optical fiber.

In the experiment, one of the six ribs, 2, was chosen and the debonding (Fig. 12) was artificially introduced in the rib. Then, a flexural wave was measured at around six FBG sensors and compared with each other for the maximum amplitudes of their first arrival waves (V_p).

Figure 14 shows the result of this experiment. In this figure, six graphs represent measured flexural waves at 1 to 6. In those graphs, dotted lines and continuous lines represent received waves and their envelopes, respectively. The envelopes were calculated with Hilbert transform. As shown in this figure, V_p measured at 2 were larger than the others. The reason of this result is as follows. Generally, if ribs and skin is bonded, wave energy in ribs of AGS diffuses to skin as the wave propagates. Since ribs and skin is debonded, it suppresses diffusion of flexural wave energy. Hence, V_p of the debonded rib became larger than those of the other ribs. Therefore, if the V_p measured in a path is larger and statistically unusual from those of the other paths, we can determine that there is a debonding along the path.

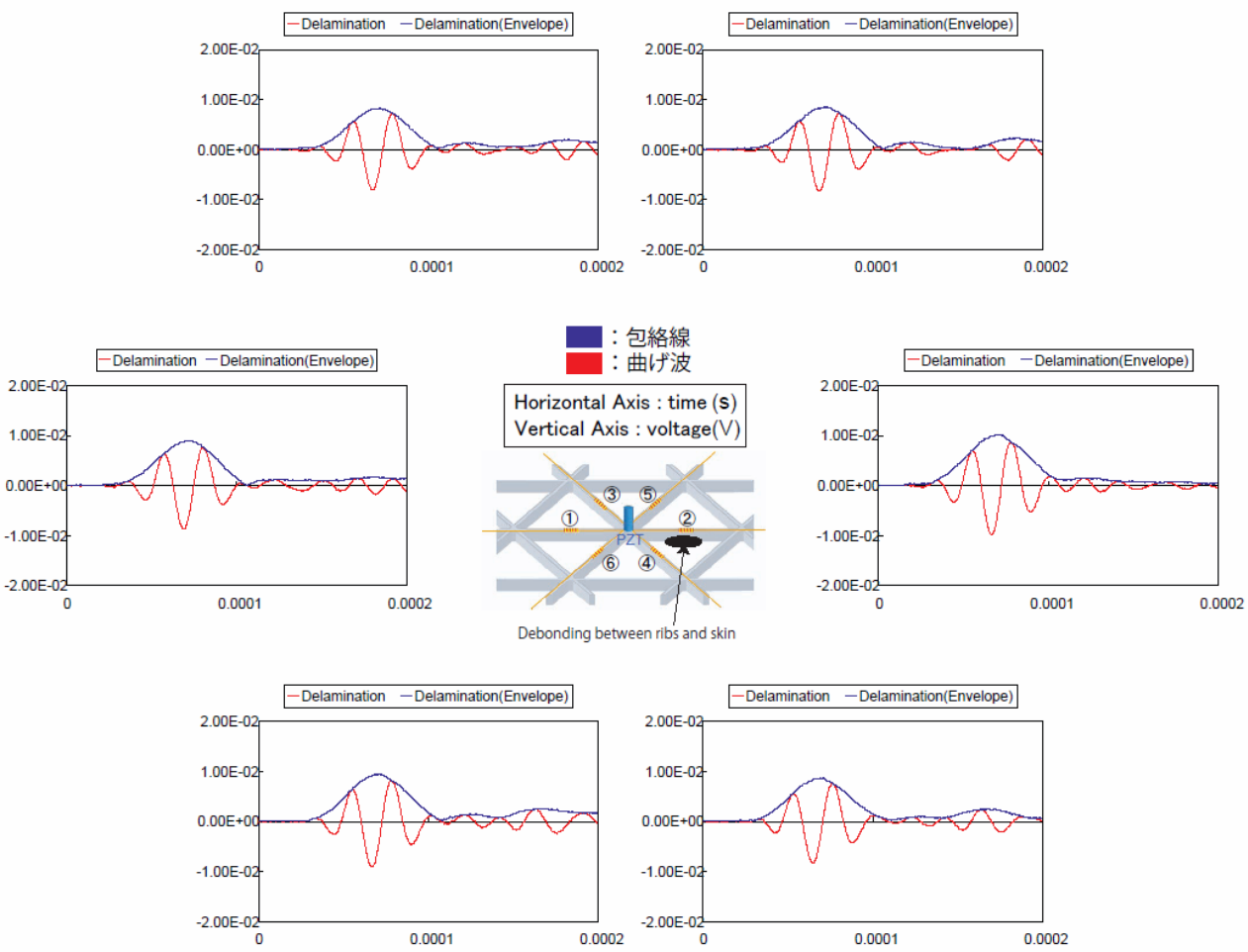

Fig. Change of the maximum amplitudes of first arrival flexural waves induced by non-adhesion between lattice and skin. The amplitudes measured at 2 increased according to non-adhesion.

5 Conclusion

In this research, we proposed a new structural health monitoring system for AGS using guided waves in ribs with the embedded FBG sensor network. Two types of guided waves, compressional and flexural waves, were taken into account for damage diagnosis. We proposed two concepts of damage diagnosis systems with compressional and flexural waves under one assumption that the mechanical characteristics of all ribs are almost identical. Therefore, if damage appears in a path, the measured wave in the path should be statistically different from those in other paths. Then, the two concepts were used for realizing two different specific damage diagnosis methods which deal with two specific damage types, rib crack and debonding between ribs and skin.

1. Propagation of compressional waves was intercepted by the generation of crack surfaces. Therefore, if the maximum amplitude of first arrival wave V_p measured in the path is smaller and statistically unusual from others, we can determine that there is a rib cracking in the path.
2. Diffusion of flexural wave energy is suppressed by the occurrence of debonding. Therefore, if the V_p of a rib is larger and statistically unusual from those of the other ribs, we can determine that the rib must be debonded.

In comparison with our previously proposed damage diagnosis methods for AGS with static strain measurement [2], these methods do not require baseline data and test loading. The two damage diagnosis methods, with static strain or with elastic waves, can be used selectively for different damage types or under different environmental conditions.

References

[1] Meyer R., Harwood O. and Orlando J. "*Isogrid design handbook*". NASA Center for AeroSpace Information (CASI), NASA-CR-124075; MDC-G4295A, 1973.

[2] Amano M., Okabe Y., Takeda N. and Ozaki T. "Structural health monitoring of advanced grid structure with embedded-fiber Bragg grating sensors". *Structural Health Monitoring*, (in press), 2007.

[3] Othonos A. and Kyriacos K. "*Fiber Bragg gratings - fundamentals and applications in telecommunications and sensing*". Arech House, Boston, London, 1999.

[4] Amano M., Arai T. and Takeda N. "Guided wave diagnosis in composite grid structure with embedded FBG sensors". *Proceedings of Smart materials and structures – an SPIE event*, San Diego, CA, 2007.

[5] Measures R. "Smart composite structures with embedded sensors". *Composites Engineering*, Vol. 2, No.5-7, pp 597-618, 1992.

[6] Ogisu T., Shimanuki M., Kiyoshima S., Okabe Y., and Takeda N. "Development of damage monitoring system for aircraft structure using a PZT actuator/FBG sensor hybrid system". *Proceedings of SPIE Smart Structures and Materials*, Vol. 5388,, pp.425-436, 2004.

[7] Uetsuka H. "AWG technologies for dense WDM applications". *IEEE JOURNAL OF SELECTED TOPICS IN QUANTUM ELECTRONICS*, Vol.10, No.2, pp.393-402, 2004.

[8] Smit M. and Dam C. "Phasar-based WDM-devices: Principles, design and applications,'" *IEEE JOURNAL OF SELECTED TOPICS IN QUANTUM ELECTRONICS*, Vol.2, No.2, pp.236-250, 1996.